PAPER

Rolled-up SiO_x/SiN_x microtubes with an enhanced quality factor for sensitive solvent sensing

To cite this article: Pengfei Song *et al* 2018 *Nanotechnology* **29** 415501

View the article online for updates and enhancements.

You may also like

- Fast prototyping of microtubes with embedded sensing elements made possible with an inkjet printing and rolling process
N Wang, M V Meissner, N MacKinnon et al.

- Review: using rolled-up tubes for strain-tuning the optical properties of quantum emitters
Gabriel Gomes, Marcos L F Gomes, Saimon F Covre da Silva et al.

- Thermal-controlled releasing and assembling of functional nanomembranes through polymer pyrolysis
Fei Ma, Borui Xu, Shuai Wu et al.

The Electrochemical Society
Advancing solid state & electrochemical science & technology

DISCOVER
how sustainability intersects with electrochemistry & solid state science research

This content was downloaded from IP address 165.124.167.1 on 12/06/2024 at 22:02

IOP Publishing Nanotechnology
Nanotechnology 29 (2018) 415501 (9pp) https://doi.org/10.1088/1361-6528/aad0b1

Rolled-up SiO_x/SiN_x microtubes with an enhanced quality factor for sensitive solvent sensing

Pengfei Song[1,2], Cheng Chen[3], Juntian Qu[1,2], Pengfei Ou[3], M H T Dastjerdi[4,5], Zetian Mi[4,6], Jun Song[3] and Xinyu Liu[1]

[1] Department of Mechanical and Industrial Engineering, University of Toronto, 5 King's College Road, Toronto, Ontario, M5S 3G8, Canada
[2] Department of Mechanical Engineering, McGill University, 817 Sherbrooke Street West, Montreal, Quebec, H3A 0C3, Canada
[3] Department of Mining and Materials Engineering, McGill University, 3610 Rue University, Montreal, Quebec, H3A 0C5, Canada
[4] Department of Electrical and Computer Engineering, McGill University, 3480 Rue University, Montreal, H3A 0E9, Canada
[5] Department of Materials Science and Engineering, Massachusetts Institute of Technology, Cambridge, MA 02139, United States of America
[6] Department Electrical Engineering and Computer Science, University of Michigan, Ann Arbor, MI 48109, United States of America

E-mail: xyliu@mie.utoronto.ca

Received 16 April 2018, revised 26 June 2018
Accepted for publication 3 July 2018
Published 3 August 2018

Abstract

The microtubes made through rolling-up of strain-engineered nanomembranes have received growing research attention after their first invention due to the technology's high flexibility, integrability, and versatility. These rolled-up microtubes have been used for a variety of device applications including sensors, batteries and transistors, among others. This paper reports the development of highly sensitive whispering-gallery mode (WGM) chemical sensors based on rolled-up microtube optical microcavities (RUM-OCs). For the first time, such microcavities were batch fabricated through rolling-up of plasma-enhanced chemical vapor deposition (PECVD)-synthesized SiO_x/SiN_x bilayer nanomembranes, which have better optical properties than the conventional electron-beam-deposited SiO/SiO_2 bilayers. Benefiting from the high refractive index (RI) of PECVD-deposited SiN_x, our RUM-OC shows an enhanced quality factor of 880 that is much higher than that (50) of a SiO/SiO_2 RUM-OC with the same dimensions. The developed RUM-OC is used for sensitive WGM solvent sensing, and demonstrate a limit of detection of 10^{-4} refractive index unit (RIU), which is 10 times lower than that (10^{-3} RIU) of a SiO/SiO_2 RUM-OC.

Supplementary material for this article is available online

Keywords: rolled-up microtube, plasma-enhanced chemical vapor deposition, optical cavity, whispering-gallery mode, chemical and biosensors

(Some figures may appear in colour only in the online journal)

 © 2018 IOP Publishing Ltd Printed in the UK

1. Introduction

Recently, microtube-based optical cavities fabricated through rolled-up nanotechnology have gained accumulated research interests thanks to their unique advantages including the nanometer-sized, subwavelength wall thickness of the microtube, excellent compatibility with on-chip integration and mass production, good material versatility and fabrication tunability [1–6]. The rolled-up nanotechnology is characterized by batch fabrication of self-assembled microtubes through release of pre-strained multi-layer nanomembranes from their mother substrate. This technology has enabled both fundamental studies and practical applications of these rolled-up microtubes [7–10]. These microtubes can serve as high-performance whispering-gallery-mode (WGM) optical resonators, and their optical resonance originates from the constructive interference of light guided within the thin wall of a microtube by total internal reflection. This phenomenon has led to a variety of applications including chemical and biosensing [6, 11–14]. Particularly, the nanometer-sized, subwavelength wall thickness of the rolled-up microtubes permits a large fraction of the WGM evanescent wave penetrating into the external environment, thereby enabling a higher sensitivity to change of the external refractive index and making it suitable for sensing applications [12, 15].

The pioneering work of developing rolled-up microtube-based optical cavities (RUM-OCs) for WGM solvent sensing was reported by Huang *et al* [12]. The authors fabricated the RUM-OC from a bilayer of electron-beam (e-beam) evaporated SiO/SiO_2 nanomembranes, and demonstrated a much higher sensitivity of 425 nm/refractive index unit (RIU) than that (typically <100 nm/RIU) of conventional WGM sensing platforms (e.g., the glass capillary). The enhanced sensitivity could be attributed to the subwavelength wall thickness (less than 100 nm) of the rolled-up microtube; however, the ultrathin wall also significantly reduces the level of light confinement. This pronounced light loss in turn shortens the photon lifetimes and broadens the resonance modes of the RUM-OC, resulting in a low quality factor (Q-factor; <100) and thus a low limit of detection (LOD) of the developed sensor [12].

Significant research efforts have been dedicated to enhancing the light confinement in rolled-up microtubes and thus improving the LOD of the optical resonance sensor [16–19]. The existing methods for improving the Q-factor of the RUM-OC are primarily based on the adjustment of the microtube structure or material composition. Among these methods, coating the inner and outer wall surfaces of the microtube with a high-refractive index material (e.g., HfO_2 or Al_2O_3) has been demonstrated to provide the maximum enhancement of the Q-factor of the RUM-OC. The Q-factor enhancement is mainly due to the coating of high-refractive index materials onto the microtube surfaces that improves the light confinement capability of the microtube [20]. RUM-OCs made from SiO/SiO_2 have been coated with HfO_2 through atomic layer deposition (ALD), and reported to have a Q-factor of up to 660 [12]. However, the employment of ALD increases the complexity and cost of microtube fabrication, and thus, to some extent, hinders the wide adoption of this method.

RUM-OCs with axial light confinement microstructures have been fabricated from high-refractive index Y_2O_3/ZrO_2 bilayer, and proved to possess a Q-factor as high as 1600 [12, 17]. Despite the high Q-factor achieved by the Y_2O_3/ZrO_2 RUM-OC, the Y_2O_3 material is toxic for human skins and model cells and is also soluble in an alcoholic environment [21], making it not suitable for certain types of biological and chemical sensing applications. In addition, Y_2O_3 absorbs light of <700 nm and thus limits the further improvement of Q-factor of the RUM-OC, as RUM-OC sensors were usually operated in the visible range (400–700 nm) [22]. Therefore, it is still necessary to seek other alternative materials, which have high-refractive indexes, good biocompatibility, and easy synthesis/fabrication processes, for batch construction of RUM-OCs with high Q-factors.

Silicon nitride (SiN_x) is non-toxic and biocompatible, and has a high-refractive index [23]; it has been widely used for constructing optical cavities and waveguides [24, 25]. Although SiN_x microtubes have been previously utilized to study neuron cells or act as inductors [26, 27], there has been no study on fabricating SiN_x-based RUM-OCs for sensing applications. It has been shown that SiN_x has a higher refractive index than that of SiO_x, promising a better light confinement capability of SiN_x-based RUM-OCs [28]. In addition, SiN_x only absorbs light at a wavelength of below 300 nm, and thereby does not lead to undesired light absorption in RUM-OCs operating in the visible wavelength range. Finally, SiN_x films can be deposited using chemical vapor deposition (CVD) techniques, which are facile and cost-effective.

In this paper, we report the fabrication, testing, and chemical sensing application of RUM-OCs made from a bilayer of SiO_x/SiN_x nanomembranes. The SiN_x layer provides a high-reflective index and thus improves the light confinement of the RUM-OCs, and the SiO_x layer provides a proper level of strain mismatch with the SiN_x layer to drive the rolling-up process. The focus of this paper is to illustrate the role of the high-reflective-index SiN_x layer in enhancing the Q-factor of the RUM-OCs; thus, we opt not to use other Q-factor improvement techniques such as ALD coating and axial light confinement structures. We demonstrate the precise control of the RUM-OC diameter by adjusting the nanomembrane thickness, providing high flexibility of the microtube fabrication. The developed RUM-OC reveals an enhanced Q-factor of up to 880, which is much higher than that of the conventional SiO/SiO_2 RUM-OC and comparable to that (660) of the previously reported HfO_2-coated SiO/SiO_2 RUM-OC. We applied our RUM-OC to solvent sensing, and achieved a LOD of 10^{-4} RIU. This result is ten times lower than that (10^{-3} RIU) of the SiO/SiO_2 RUM-OC.

2. Microtube fabrication

The SiO_x/SiN_x microtubes were fabricated through controlled release of strain-engineered bilayer SiO_x/SiN_x nanomembranes. The strain difference between the SiO_x and SiN_x

layers is the driving force for the self-rolling of the nanomembranes. The value of the strain difference needs to be above a certain threshold to roll the bilayer nanomembranes into a tubular microstructure rather than forming non-tubular substrates such as wrinkles or buckles [29]. Therefore, the prerequisite of microtube rolling-up is to determine a suitable strain difference value between the SiO_x and SiN_x layers. As the SiN_x film was the major layer we investigated, we directly used the standard recipe provided by our microfabrication facility for SiO_x deposition (see details below), and only tuned the deposition parameters for SiN_x to achieve two objectives: (1) to determine the optimal strain difference between the SiO_x and SiN_x layers and obtain the highest yield of microtube rolling-up, (2) to maintain a high-refractive index of SiN_x (as the reflective index of SiN_x is also affected by the deposition parameters).

There are several parameters to tune for the SiN_x deposition, including the deposition power, frequency, temperature, and the SiH_4/NH_3 gas ratio. These parameters all could affect the built-in stress and the refractive index of the deposited SiN_x film. In order to simplify the experiment, we only tuned the SiH_4/NH_3 gas ratio with other parameters fixed (70 W, 13.56 MHz, and 300 °C). We chose to only tune the SiH_4/NH_3 gas ratio because it is the most commonly adjusted parameter during PECVD deposition of SiN_x films and has been extensively studied [23, 25, 30]. It was commonly observed that, with the increase of SiH_4/NH_3 gas ratio, the refractive index of deposited SiN_x film became higher (which yielded better light confinement of the optical cavity) while the built-in tensile stress of the film became smaller (which compromised the rolling-up process) [23, 30, 31]. This result could be explained by that the higher SiN_x flow leads to the larger Si-incorporation in the deposited film, creating the so-called 'Si-rich' film and thereby the higher refractive index and lower tensile stress. Fourier-transform infrared spectroscopy (FTIR) measurements shows the increase of Si–H bonds and the decrease of N–H bonds [23], which supports this explanation. Therefore, a balanced SiH_4/NH_3 gas ratio needs to be experimentally determined. Maintaining the NH_3 flow rate at a common level of 10 standard cubic centimeter per minute (sccm), we used three typical SiH_4/NH_3 volume ratios (1, 2, and 3) to deposit the SiN_x films, and examined the rolling-up yield of the SiO_x/SiN_x bilayer nanomembranes with the same in-plane pattern. We achieved the highest rolling-up yield of 99% ($n = 300$) at the gas ratio of 1, and thereby the flow rate of 10 sccm for both SiH_4 and NH_3 was used in the following experiments.

As shown in figure 1(A-i), the fabrication process started from e-beam deposition (equipment: BJD 1800, Temescal) of an aluminum (Al) sacrificial layer (50 nm) on a pre-cleaned three-inch silicon wafer. We chose Al as the sacrificial layer because of its highly selective wet etching over SiO_x/SiN_x and its low surface roughness (<1.25 nm) [32]. The SiO_x/SiN_x (bottom/top) bilayer nanomembranes were then deposited by PECVD (equipment: Plasmalab System100, Oxford Instruments). The following gas flow parameters of PECVD were used: (i) 8.5 sccm of SiH_4 and 710 sccm of N_2O for SiO_2 deposition, and (ii) 10 sccm of SiH_4 and 10 sccm of NH_3 for SiN_x deposition. These parameters ensured the suitable stress difference for driving the rolling-up of microtubes (see details in the section of 'analysis of microtube diameter tunability'). The deposition temperature, power, and frequency were maintained at 300 °C, 70 W, and 13.56 MHz for deposition of both SiO_x and SiN_x layers.

The SiO_x/SiN_x bilayers were then patterned into a U-shape (figure 1(A-ii)) through standard photolithography (etch mask: 1.4 μm thick S1813, and SiO_x/SiN_x etchant: 4.9% hydrofluoric acid). After that, rectangular photoresist strips were patterned to cover the legs of the U-shaped SiO_x/SiN_x nanomembranes (figure 1(A-iii)), which anchored rolled-up microtubes to the substrate during the releasing process. The SiO_x/SiN_x nanomembranes were released from their substrate using an aluminum etchant (type-A, Transene Inc.) at 60 °C, during which the SiO_x/SiN_x bilayers self-rolled once the sacrificial Al layer was etched off (figure 1(A-iv)). Once the rolling-up process was completed, the anchoring photoresist strips were removed. The sample wafer was immersed in DI water, and then in 200-proof isopropyl alcohol (IPA) three times with 20 min immersion for each time. Finally, the sample wafer was dried in a CO_2 critical point dryer (Autosamdri®-815, Tousimis). Figure 1(B) shows an array of rolled-up microtubes with the anchor photoresist removed. The final fabrication yield was determined to be 99% ($n = 300$).

3. Analysis of microtube diameter tunability

In addition to the high rolling-up yield of the microtubes, the tunability of the microtube diameter is also critical for optimizing the sensor performance as it determines the light-path length of the WGM resonance cycle. The good tunability and reproducibility of the microtube diameter are highly desired. To gain insights about the deterministic factors of the microtube diameter, the rolling-up process of the microtube was first theoretically analyzed within the framework of continuum mechanics [33]. Compared to the conventional analytical model of the microtube rolling-up [33], we developed a new model that considers, for the first time, the effects of the longitudinal and transverse mismatch strains simultaneously. The new model can be used to more accurately calculate the curvature κ of a thin-film bilayer with mismatched strains ε_0 and $\eta\varepsilon_0$ along the longitudinal and transverse directions respectively. The details of the model derivation can be found in a separate paper [34]. Briefly, this model was derived from the Von-Karman plate theory [35, 36] and Rayleigh–Ritz model [35, 37, 38], and accounts for the anisotropic lattice mismatch coefficient η. Note that, in the particular case of $\eta = 0$, equation (1) below simplifies to the Timoshenko formula [39] which was employed by previous studies to predict the roll-up curvature [40, 41]. In our calculations, the mechanical properties of SiO_x/SiN_x were taken as $(E_b, E_t) = (72.2, 175)$ GPa, $\nu = 0.25$ [42]. Here, we provide the final derived equation of the microtube curvature

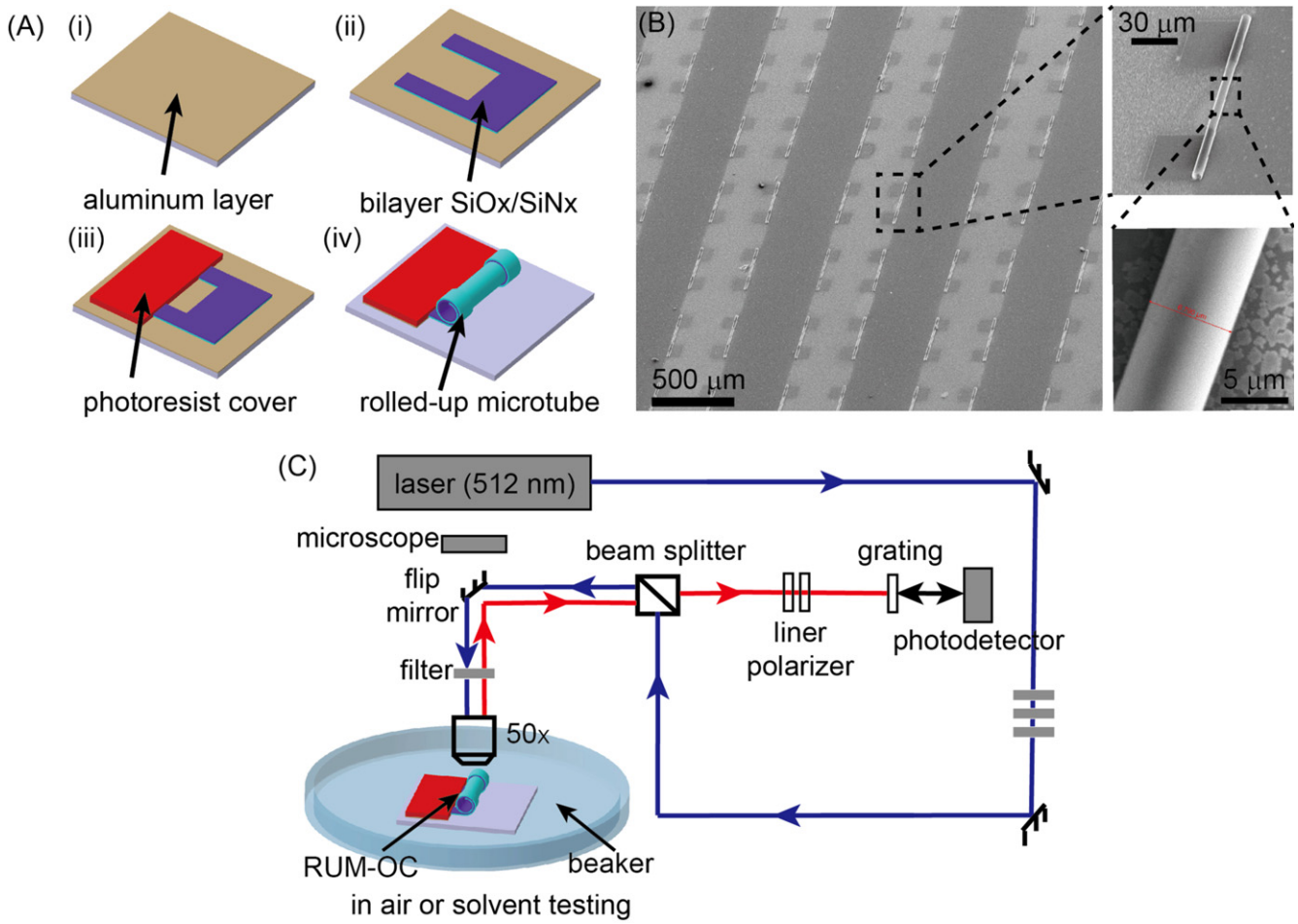

Figure 1. (A) Schematic views of the rolled-up microtube fabrication process. (B) SEM image of a rolled-up microtube array and zoomed-in views of a single microtube. (C) Schematic setup for photoluminescence measurement on a rolled-up microtube.

(the reciprocal of the microtube radius):

$$\kappa = \frac{6 \cdot \varepsilon_0 \cdot E_b \cdot E_t \cdot h_b \cdot h_t (h_b + h_t)(1 + \eta\nu)}{E_b^2 h_t^4 + 4h_b \cdot h_t \left(h_b^2 + \frac{3}{2} h_t \cdot h_b + h_t^2\right) E_b \cdot E_t + E_t^2 h_t^4}, \quad (1)$$

where the bottom and top layers are respectively of Young's moduli (E_b, E_t), thicknesses (h_b, h_t), and the same Poisson ratio ν. The most straightforward way of tuning the microtube diameter is to adjust the thicknesses (h_b, h_t) of the two nanomembrane layers because the Young's moduli and Poisson ratio are independent of the film thickness [43].

We also experimentally demonstrated that the built-in stresses (ε_0 and $\eta\varepsilon_0$) of the SiO_x and SiN_x nanomembranes are also independent of the nanomembrane thicknesses. We measured the built-in stresses of SiO_x and SiN_x nanomembranes using a film stress measurement system (Flexus 5200, Tencor). The results showed repeatable built-in stresses of -831.5 ± 21.4 MPa ($n = 20$; compressive stress) for SiO_x films of four different thicknesses (15, 25, 35 and 45 nm; five measurements for each thickness) and 221.5 ± 12.1 MPa ($n = 15$; tensile stress) for SiN_x films of three different thicknesses (10, 20 and 30 nm; five measurements for each thickness). Thus, by adjusting the nanomembrane thicknesses, we fabricated microtubes with diameters of 3.9–16.1 μm. A scanning electron microscope (SEM, FEI 50) was used to measure the microtube diameter. Figure 2 shows the theoretically predicted (through equation (1)) and experimentally measured microtube diameters as functions of the top (SiN_x) and bottom (SiO_x) layer thicknesses. One can see that our developed model accurately predicts the microtube diameter based on the different combination of the nanomembrane thicknesses, and thus can be used for guiding future microtube designs. In addition, the measured microtube diameter for each combination of nanomembrane thicknesses shows a small variation (<0.5 μm; $n = 10$), confirming that the microtube diameter can be well-controlled with high reproducibility.

4. Photoluminescence characterization of microtube

The WGM resonance performance of the fabricated RUM-OC was characterized at room temperature using a photoluminescence (PL) microscope (InVia 3000, Renishaw). An

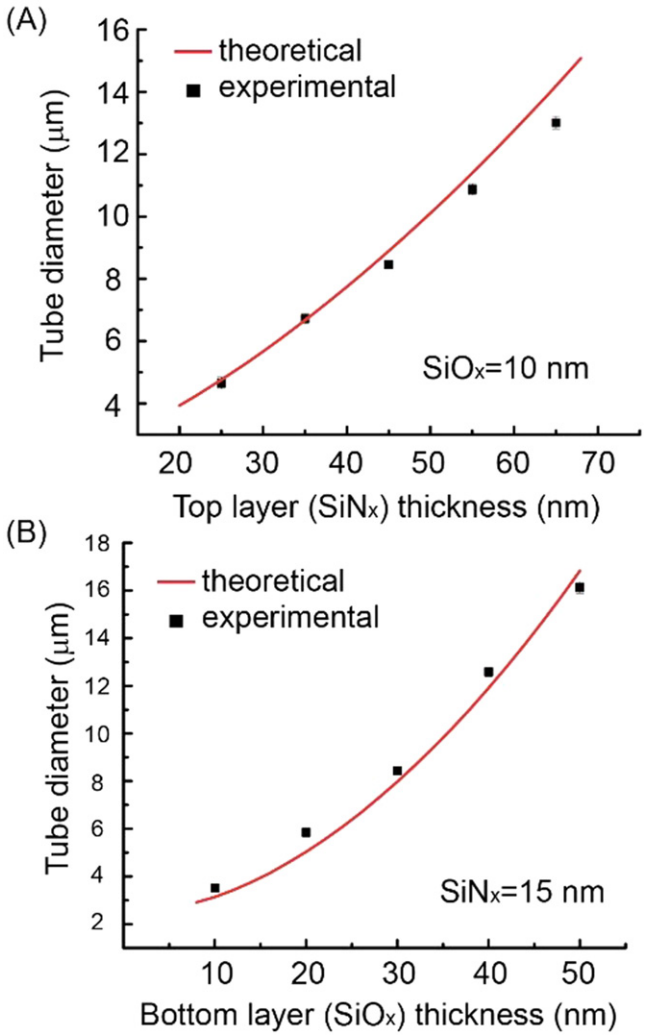

Figure 2. The microtube diameter as a function of (A) SiN_x and (B) SiO_x thicknesses (with the thickness of another layer fixed). The theoretically predicated diameters (red lines) are in good agreement with the experimentally measured values (black dots; $n = 10$).

excitation line at 514 nm was used and the emission spectrum was collected through a 50× objective (numerical aperture: 0.55). The Q-factor of a resonance mode is calculated as $Q = \lambda/\Delta\lambda$, where the λ is the mode position and $\Delta\lambda$ is the full width at half maximum of the mode [12].

As shown in figure 3(A), the PL spectrum collected from the center spot of a RUM-OC (6.8 μm diameter, 10 nm SiO_x and 35 nm SiN_x) showed a broad emission band, which was due to the emission from defect centers inside the SiO_x/SiN_x layers [5]. The modulation of the PL intensity by the tubular structure was also clearly observed, which was contributed by the WGM resonance in the tubular structure of the RUM-OC. The WGM resonance modes were polarized in parallel with the microtube axis, corresponding to the transverse magnetic (TM) modes. No clear transverse electric polarization was observed in the PL spectrum due to the lack of axial optical confinement structure in our microtube design [44].

To analyze the observed resonance modes, the azimuthal mode number M was calculated by $M = n_{eff}\frac{d}{\lambda}$, where n_{eff} is the effective refractive index of the microtube wall material and the surrounding medium penetrated by the evanescent field of the guided light, d is the microtube diameter, and λ is the wavelength of the mode. The effective refractive index n_{eff} can be calculated using $n_{eff} = x \cdot n_{SiO_x} + (1 - x) \cdot n_{SiN_x}$, where x is the filling ratio of each material for constructing the microtube. For our RUM-OC, n_{eff} was calculated to be 1.86. The Q-factor was then calculated for each mode by extracting the value of $\Delta\lambda$ using Lorenz fitting, and the highest Q-factor was determined to be 880 at mode 39. This Q-factor is much higher than the reported value (~100) of non-HfO_2-coated SiO/SiO_2 RUM-OCs [44], and is comparable to that (660) of HfO_2-coated SiO/SiO_2 RUM-OCs [12]. We also fabricated SiO/SiO_2 RUM-OCs using e-beam evaporation (without HfO_2 coating) with the same microtube diameter (6.8 μm) and the same total microtube wall thickness (45 nm; 10 nm for SiO and 35 nm for SiO_2), and compared their Q-factor with that of our SiO_x/SiN_x RUM-OC. Figure 3(B) shows a typical PL spectrum measured on a SiO/SiO_2 RUM-OC. The highest Q-factor of the SiO/SiO_2 RUM-OC was measured to be 50, which is much lower than that of our SiO_x/SiN_x RUM-OC.

The enhanced Q-factor of our SiO_x/SiN_x RUM-OC is mainly due to the higher refractive index of the SiN_x film in the visible range over that of the SiO_2 film, which was confirmed by our ellipsometry measurement results shown in figures 3(C) and (D). One can see that the refractive index of SiN_x was measured to be ~66.7% higher than that of the SiO_x. Although the Q-factor is still lower than the previously reported value of Y_2O_3/ZrO_2 RUM-OC [17], the low light absorption of our SiO_x/SiN_x RUM-OC promises further improvement of its Q-factor by using various techniques such as ALD HfO_2 coating [12] and axial light confinement structures [19].

5. Solvent sensing experiments

As a proof-of-concept demonstration, we used the developed SiO_x/SiN_x RUM-OC for solvent sensing. During optical resonance in the RUM-OC, the WGM evanescent wave penetrates the RUM-OC wall and interacts with its surrounding medium. Once the optical property of the external environment changes, the altered interaction between the WGM evanescent wave and the surrounding medium leads to a detectable change of WGM resonance spectrum; thus, the detection of the surrounding medium of the RUM-OC can be realized. The subwavelength wall thickness of the RUM-OC makes it particularly suitable for medium sensing applications, as the large fraction of the WGM evanescent interacts with the external medium, and thereby promises an enhanced sensitivity.

In the sensing experiments, we measured the PL spectra of the RUM-OC in two different solvents: DI water and ethanol, and compared the measured spectra with the background spectrum of the RUM-OC measured in air (relatively humidity: 40%). The RUM-OCs used in the experiments have a diameter of 6.8 μm and a wall thickness of 45 nm (10 nm for SiO_x and 35 nm for SiN_x). The PL spectra were collected

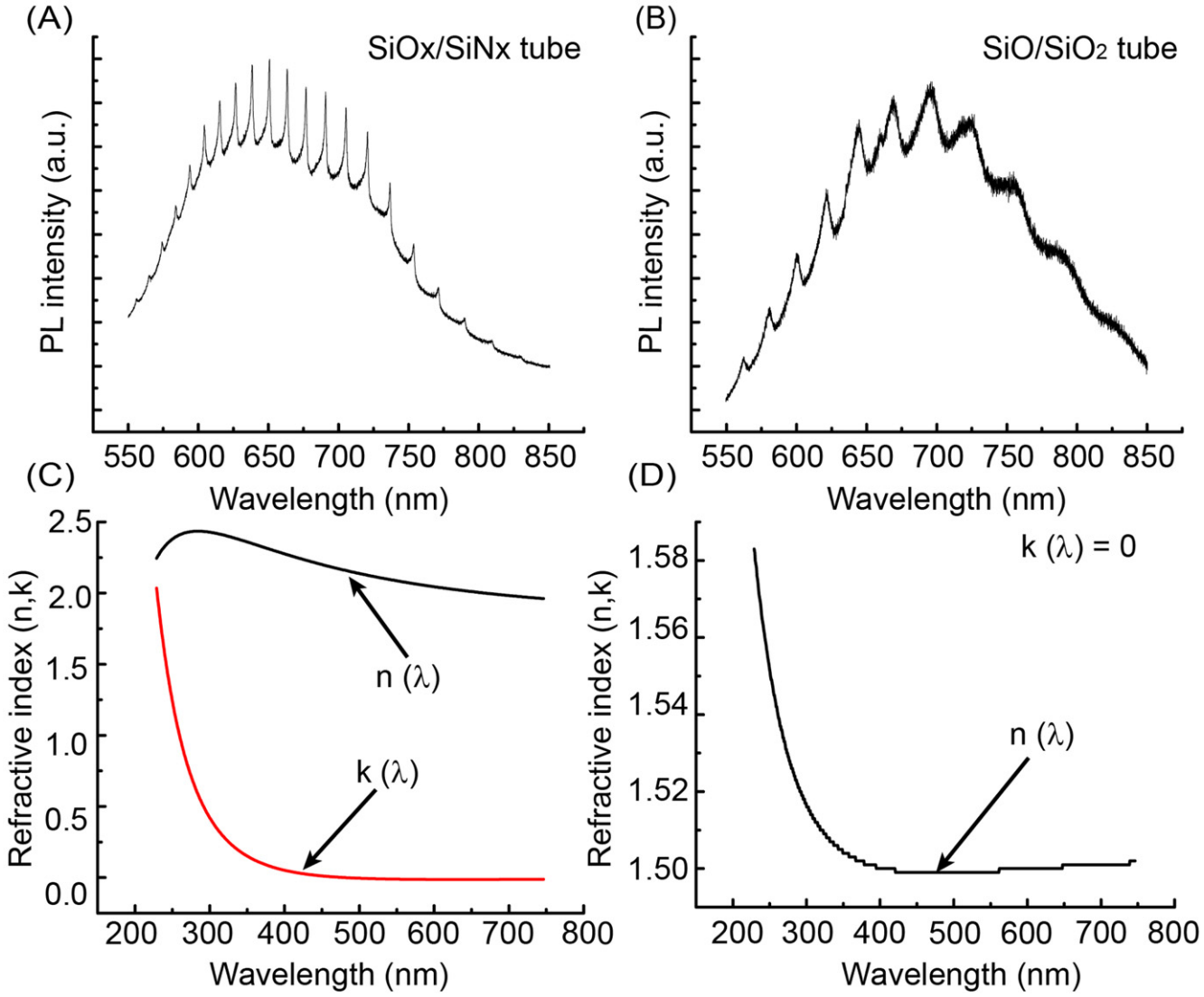

Figure 3. (A), (B) Photoluminescence (PL) spectra of (A) a SiO_x/SiN_x RUM-OC made by PECVD and (B) a SiO/SiO_2 RUM-OC made by e-beam deposition. The intensity of each spectrum is normalized against its strongest mode. (C), (D) Ellipsometry measurement results of the complex refractive indices of (C) SiN_x and (D) SiO_2 thin-films. $k(\lambda)$ and $n(\lambda)$ are the absorption coefficient and refractive index, respectively.

at room temperature using the same 50× objective and excitation line at 514 nm. Figure 4(A) shows the PL spectra of the RUM-OCs in DI water, ethanol, and air. The WGM resonance was observed in the spectra measured in all the three different environments, but with clear differences. Specifically, a red shift of the spectrum occurred once the RUM-OC was immersed into a solvent due to the higher refractive index of the new medium than air. This observation can be explained by this simplified equation: $2\pi R \cdot n_{eff} \approx M \cdot \lambda$. For the same mode number M, the λ increases with n_{eff} (the effective reflective index of the microtube wall and the surrounding medium).

To quantify the sensing performance of the developed RUM-OC, the analytical mode positions (based on the mature analytical method [12]) were calculated. The resonant TM modes of an optical cavity can be analyzed by the following equation with waveguide approximation [12]:

$$\tan(\gamma h) = \frac{2\delta/\gamma}{1 - (\delta/\gamma)^2}, \tag{2}$$

where $\delta = \sqrt{(2m/d)^2 - \varepsilon_2(2\pi/\lambda_0)^2}$, $\gamma = \sqrt{\varepsilon_1(2\pi/\lambda_0)^2 - (2m/d)^2}$, h and d are the tube thickness and diameter respectively, m is the azimuthal mode number, and ε_1 and ε_2 are the dielectric constants of the microtube wall and surrounding medium respectively. In our calculations, due to the centrosymmetric tube structure, the rolled-up microtube was treated as a slab and no surface curvature effects and notches at the rolling edge of the tube were considered. This treatment simplified it into a two-dimensional problem. The effective thickness h and the dielectric constant ε_1 of the microtube wall were obtained by combining the thickness and dielectric constant of the SiO_x and SiN_x layers (which constitute the microtube wall), respectively,

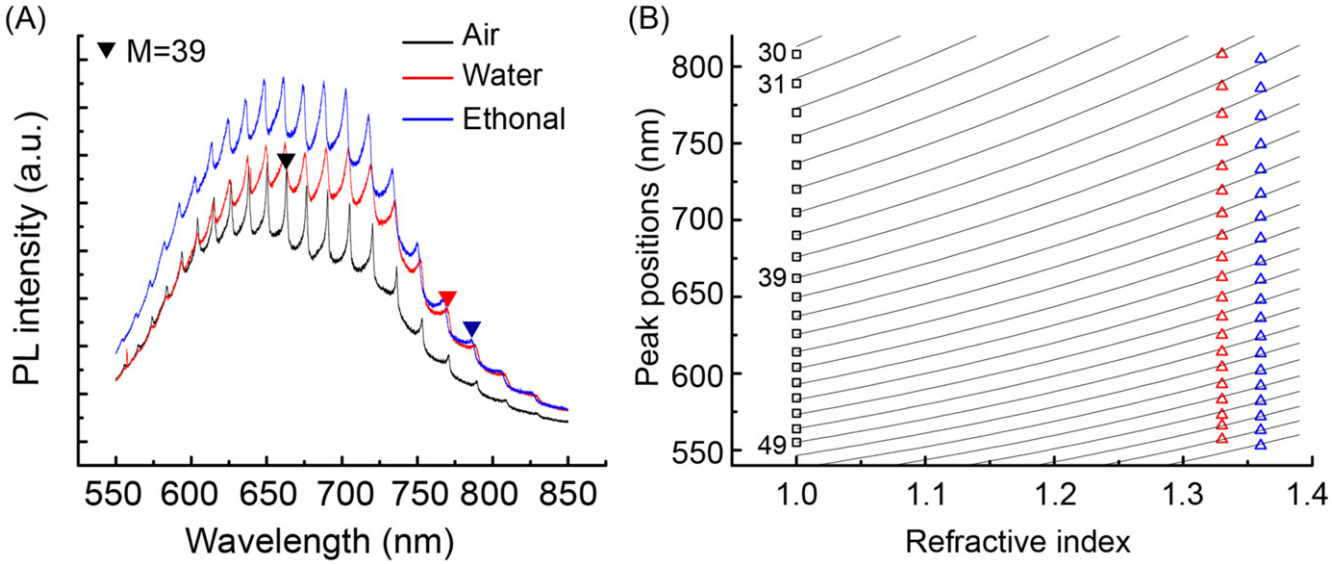

Figure 4. (A) PL spectra of rolled-up microtubes in different solvents. (B) Peak position of the TM mode as a function of refractive index of surrounding medium. The solid lines are predicted values, and the black, blue, and red triangles represent experimental mode positions in air, water, and ethanol solution, respectively.

using the method derived in [12]. The detailed calculations can be found in the supplementary material available online at stacks.iop.org/NANO/29/415501/mmedia.

The theoretically calculated position shifts and experimental data were shown in figure 4(B). It can be seen that the calculated position shifts agree well with the measured data. The sensitivity of the RUM-OC can thereby be determined by

$$S = \frac{\lambda_{M,ethanol} - \lambda_{M,water}}{n_{ethonal} - n_{water}}, \quad (3)$$

where $\lambda_{M,ethanol}$ and $\lambda_{M,water}$ represent the TM mode positions for the same azimuthal number M in ethanol and water, respectively. The $n_{ethonal} = 1.36$ and $n_{water} = 1.33$ are the refractive indices of ethanol and water, respectively. The highest sensitivity was determined to be 510 nm/RIU at mode 3. This result is consistent with the analytical calculation showing that a smaller azimuthal number mode possesses a higher sensitivity.

The LOD is another important parameter of the RUM-OC sensor, and can be estimated by

$$\mathrm{LOD} = \frac{3\sigma}{S}, \quad (4)$$

where σ is the standard deviation of the system noise and S is the value of the sensitivity. The system noise σ of the RUM-OC was primarily contributed by statistical distributions of the peak position measurements, and could be approximated by $\sigma = \Delta\lambda/50$, where the $\Delta\lambda$ is the line width [12]. We chose the PL peak at 660 nm ($M = 39$), with $\Delta\lambda = 0.75$ nm, as it provided the highest *Q-factor* and thereby the best LOD among all the WGM supporting modes in our RUM-OC. The obtained LOD of our RUM-OC is in the order of 10^{-4} RIU, which is 10 times lower than that (10^{-3} RIU) of the HfO_2-coated SiO/SiO_2 RUM-OC [12]. The improved LOD was contributed by the high *Q-factor* of the WGM supporting mode at $M = 39$. The LOD improvement could be explained by that the light loss during the WGM resonance within the ultrathin wall was reduced by the high-refractive index of SiN_x. The enhanced light confinement of the microtube wall prolonged the photon lifetimes, and thereby increased the quality factor, resulting in the improved LOD of the developed sensors.

6. Conclusion

By adopting a new material combination of SiO_x and SiN_x, we successfully fabricated RUM-OCs with an enhanced *Q*-factor and applied them to sensitive solvent sensing. The SiN_x material featured high-refractive index and zero light absorption in the visible range, and thus provided good light confinement capability for the SiO_x/SiN_x RUM-OC. The PECVD technique used for synthesizing SiO_x and SiN_x allowed facile tuning of the thicknesses and build-in stresses of the SiO_x/SiN_x bilayers, thus leading to precise and reproducible control of the RUM-OC diameter. Benefiting from the good light confinement capability of SiN_x, our RUM-OC provided a *Q*-factor of up to 880, which is comparable to that (660) of the previously reported HfO_2-coated SiO/SiO_2 RUM-OC and much higher than that (50) of the non-coated SiO/SiO_2 RUM-OC. For solvent sensing, our SiO_x/SiN_x RUM-OC revealed a sensitivity of 510 nm/RIU and a LOD in the order of 10^{-4} RIU. The LOD of our SiO_x/SiN_x RUM-OC is 10 times lower than that (10^{-3} RIU) of the HfO_2-coated SiO/SiO_2 RUM-OC.

Acknowledgments

This research was supported by the Natural Sciences and Engineering Research Council of Canada (NSERC) (grant numbers: STPGP/463182-2014, RGPIN-06374-2017, and RGPAS-507980-2017). The authors also acknowledge the financial support from the Canada Research Chairs Program

(grant no. 237293) to X Liu, from the Chinese Scholarship Council to P Song and C Chen, and from CMC Microsystems (for device microfabrication) to P Song. The authors also thank Dr Sasa Ristic at the McGill Nanotools Microfab Facility and Dr Di Han from Fudan University, China for their discussions.

ORCID iDs

Cheng Chen https://orcid.org/0000-0003-3062-9048
Juntian Qu https://orcid.org/0000-0002-1799-5847
Xinyu Liu https://orcid.org/0000-0001-5705-9765

References

[1] Mei Y, Huang G, Solovev A A, Urena E B, Mönch I, Ding F, Reindl T, Fu R K, Chu P K and Schmidt O G 2008 Versatile approach for integrative and functionalized tubes by strain engineering of nanomembranes on polymers *Adv. Mater.* **20** 4085–90

[2] Harazim S M, Xi W, Schmidt C K, Sanchez S and Schmidt O G 2012 Fabrication and applications of large arrays of multifunctional rolled-up SiO/SiO_2 microtubes *J. Mater. Chem.* **22** 2878–84

[3] Lin X, Fang Y, Zhu L, Zhang J, Huang G, Wang J and Mei Y 2016 Self-rolling of oxide nanomembranes and resonance coupling in tubular optical microcavity *Adv. Opt. Mater.* **4** 936–42

[4] Wang J, Zhan T, Huang G, Chu P K and Mei Y 2014 Optical microcavities with tubular geometry: properties and applications *Laser Photon. Rev.* **8** 521–47

[5] Songmuang R, Rastelli A, Mendach S and Schmidt O G 2007 SiO_x/Si radial superlattices and microtube optical ring resonators *Appl. Phys. Lett.* **90** 091905

[6] Zhang Y, Han D, Du D, Huang G, Qiu T and Mei Y 2015 Rolled-up Ag–SiO_x hyperbolic metamaterials for surface-enhanced raman scattering *Plasmonics* **10** 949–54

[7] Schmidt O G and Eberl K 2001 Nanotechnology: thin solid films roll up into nanotubes *Nature* **410** 168

[8] Mi Z and Bianucci P 2012 When self-organized In(Ga)As/GaAs quantum dot heterostructures roll up: emerging devices and applications *Curr. Opin. Solid State Mater. Sci.* **16** 52–8

[9] Dastjerdi M, Djavid M and Mi Z 2015 An electrically injected rolled-up semiconductor tube laser *Appl. Phys. Lett.* **106** 021114

[10] Zhong Q, Tian Z, Dastjerdi M H T, Mi Z and Plant D V 2013 Counterpropagating whispering-gallery-modes of rolled-up semiconductor microtubes *IEEE Photon. Technol. Lett.* **25** 1691–4

[11] Harazim S M, Quiñones V A B, Kiravittaya S, Sanchez S and Schmidt O G 2012 Lab-in-a-tube: on-chip integration of glass optofluidic ring resonators for label-free sensing applications *Lab Chip* **12** 2649–55

[12] Huang G, Bolaños Quiñones V A, Ding F, Kiravittaya S, Mei Y and Schmidt O G 2010 Rolled-up optical microcavities with subwavelength wall thicknesses for enhanced liquid sensing applications *ACS Nano* **4** 3123–30

[13] Zhong J, Wang J, Huang G, Yuan G and Mei Y 2013 Effect of physisorption and chemisorption of water on resonant modes of rolled-up tubular microcavities *Nanoscale Res. Lett.* **8** 1–6

[14] Han D, Fang Y, Du D, Huang G, Qiu T and Mei Y 2016 Automatic molecular collection and detection by using fuel-powered microengines *Nanoscale* **8** 9141–5

[15] Zhao F, Zhan T, Huang G, Mei Y and Hu X 2012 Liquid sensing capability of rolled-up tubular optical microcavities: a theoretical study *Lab Chip* **12** 3798–802

[16] White I M and Fan X 2008 On the performance quantification of resonant refractive index sensors *Opt. Express* **16** 1020–8

[17] Wang J, Zhan T, Huang G, Cui X, Hu X and Mei Y 2012 Tubular oxide microcavity with high-index-contrast walls: Mie scattering theory and 3D confinement of resonant modes *Opt. Express* **20** 18555–67

[18] Böttner S, Li S, Jorgensen M R and Schmidt O G 2013 Vertically aligned rolled-up SiO_2 optical microcavities in add-drop configuration *Appl. Phys. Lett.* **102** 251119

[19] Böttner S, Li S, Trommer J, Kiravittaya S and Schmidt O G 2012 Sharp whispering-gallery modes in rolled-up vertical SiO_2 microcavities with quality factors exceeding 5000 *Opt. Lett.* **37** 5136–8

[20] Wang J, Huang G and Mei Y 2014 Modification and resonance tuning of optical microcavities by atomic layer deposition *Chem. Vapor Depos.* **20** 103–11

[21] Selvaraj V, Bodapati S, Murray E, Rice K M, Winston N, Shokuhfar T, Zhao Y and Blough E 2014 Cytotoxicity and genotoxicity caused by yttrium oxide nanoparticles in HEK293 cells *Int. J. Nanomed.* **9** 1379–91

[22] Nigara Y 1968 Measurement of the optical constants of yttrium oxide *Japan. J. Appl. Phys.* **7** 404

[23] Karouta F, Vora K, Tian J and Jagadish C 2012 Structural, compositional and optical properties of PECVD silicon nitride layers *J. Phys. D: Appl. Phys.* **45** 445301

[24] Ghulinyan M, Pitanti A, Pucker G and Pavesi L 2009 Whispering-gallery mode micro-kylix resonators *Opt. Express* **17** 9434–41

[25] Gorin A, Jaouad A, Grondin E, Aimez V and Charette P 2008 Fabrication of silicon nitride waveguides for visible-light using PECVD: a study of the effect of plasma frequency on optical properties *Opt. Express* **16** 13509–16

[26] Huang W, Yu X, Froeter P, Xu R, Ferreira P and Li X 2012 On-chip inductors with self-rolled-up SiN_x nanomembrane tubes: a novel design platform for extreme miniaturization *Nano Lett.* **12** 6283–8

[27] Froeter P, Huang Y, Cangellaris O V, Huang W, Dent E W, Gillette M U, Williams J C and Li X 2014 Toward intelligent synthetic neural circuits: directing and accelerating neuron cell growth by self-rolled-up silicon nitride microtube array *ACS Nano* **8** 11108–17

[28] Kim D, Yoon S, Jang G, Suh S, Kim H and Yoon D 2006 Refractive index properties of SiN thin films and fabrication of SiN optical waveguide *J. Electroceramics* **17** 315–8

[29] Cendula P, Malachias A, Deneke C, Kiravittaya S and Schmidt O G 2014 Experimental realization of coexisting states of rolled-up and wrinkled nanomembranes by strain and etching control *Nanoscale* **6** 14326–35

[30] Mackenzie K, Johnson D, DeVre M, Westerman R and Reelfs B 2005 Stress control of Si-based PECVD dielectrics *Proc. 207th Electrochemical Society Meeting* pp 148–59

[31] Iliescu C, Tay F E and Wei J 2006 Low stress PECVD—SiN_x layers at high deposition rates using high power and high frequency for MEMS applications *J. Micromech. Microeng.* **16** 869

[32] Bordo K and Rubahn H-G 2012 Effect of deposition rate on structure and surface morphology of thin evaporated Al films on dielectrics and semiconductors *Mater. Sci.* **18** 313–7

[33] Grundmann M 2003 Nanoscroll formation from strained layer heterostructures *Appl. Phys. Lett.* **83** 2444–6

[34] Chen C, Song P, Meng F, Li X, Liu X and Song J 2017 Quantitative analysis and predictive engineering of self-rolling of nanomembranes under anisotropic mismatch strain *Nanotechnology* **28** 485302

[35] Freund L B 2000 Substrate curvature due to thin film mismatch strain in the nonlinear deformation range *J. Mech. Phys. Solids* **48** 1159–74

[36] Vidoli S 2013 Discrete approximations of the Foppl–Von Karman shell model: from coarse to more refined models *Int. J. Solids Struct.* **50** 1241–52

[37] Dano M L and Hyer M W 1998 Thermally-induced deformation behavior of unsymmetric laminates *Int. J. Solids Struct.* **35** 2101–20

[38] Hyer M W 1981 Calculations of the room-temperature shapes of unsymmetric laminates *J. Compos. Mater.* **15** 296–310

[39] Timoshenko S 1925 Analysis of bi-metal thermostats *J. Opt. Soc. Am. Rev. Sci.* **11** 233–55

[40] Zang J and Liu F 2008 Modified Timoshenko formula for bending of ultrathin strained bilayer films *Appl. Phys. Lett.* **92** 021905

[41] Li X L 2008 Strain induced semiconductor nanotubes: from formation process to device applications *J. Phys. D: Appl. Phys.* **41** 193001

[42] Froeter P, Yu X, Huang W, Du F, Li M Y, Chun I, Kim S H, Hsia K J, Rogers J A and Li X L 2013 3D hierarchical architectures based on self-rolled-up silicon nitride membranes *Nanotechnology* **24** 475301

[43] Huang W, Koric S, Yu X, Hsia K J and Li X 2014 Precision structural engineering of self-rolled-up 3D nanomembranes guided by transient quasi-static FEM modeling *Nano Lett.* **14** 6293–7

[44] Quiñones V A B 2014 Rolled-up microtubular cavities towards three-dimensional optical confinement for optofluidic microsystems *PhD Thesis* Chemnitz University of Technology